In Situ Study of the Effect of the Exposed Surface of Ceria (100 vs 111) on the Highly Oxidized Species Formation on Ru/Ceria Catalysts

O. Bezkrovnyi[a,*], P. Kraszkiewicz[a] and M. Vorochta[b]

[a] *W. Trzebiatowski Institute of Low Temperature and Structure Research, Polish Academy of Sciences, 50-422 Wroclaw, Poland*
[b] *Department of Surface and Plasma Science, Faculty of Mathematics and Physics, Charles University, V Holešovičkách 2, 180 00, Prague 8, Czech Republic*

Received: 18.01.2024 & Accepted: 04.04.2024

Doi: 10.12693/APhysPolA.145.310 *e-mail: o.bezkrovnyi@intibs.pl

In-depth recognition of chemical processes that occur in Ru/CeO_2 catalysts under realistic reaction conditions of C_3H_8 oxidation was studied using the near-ambient pressure X-ray photoelectron spectroscopy technique. The relevance of the proposed study is based on the wide use of ceria-based catalysts in industrially relevant red–ox reactions for reducing volatile organic compound emissions. Primary attention was paid to the effect of the exposed face of CeO_2 support ((100) or (111)) on the formation of highly oxidized Ru species (volatile RuO_4), which are decisively responsible for the Ru loss and thus deactivation of Ru-based catalysts.

topics: ceria, ruthenium, oxidation, near-ambient pressure X-ray photoelectron spectroscopy (NAP-XPS)

1. Introduction

Ru-based ceria-supported materials are widely used catalysts for the total oxidation of volatile organic compounds (VOCs), which are dangerous to humans as they cause various health problems. Two key factors are responsible for the catalytic activity of Ru/CeO_2 catalysts [1]. The first one is reversible Ce^{4+}/Ce^{3+} transitions in ceria [2]. This process determines the ability of ceria-based catalysts to transport oxygen to the active sites, an essential step in Mars–van Krevelen (MvK) reaction mechanism. The second one is the chemical state of Ru sites, a crucial factor in both MvK and Langmuir–Hinshelwood (LH) reaction mechanisms. Considering that the working temperatures during the processes of VOCs oxidation may vary over an extensive range (150–400°C), changes in the chemical state of the Ru in Ru/CeO_2 catalyst are very likely [3–6]. In our previous work, we showed for the first time that Ru^{8+} is formed (as a volatile RuO_4) during exposure of Ru/CeO_2 to an oxygen-rich atmosphere at elevated temperatures [7].

The present work aims to study the chemical interaction between Ru and CeO_2 in a Ru/CeO_2 catalyst under the real conditions of C_3H_8 oxidation. Propane was chosen as a model VOC, which contains C–C and C–H bonds, and its oxidation can simulate, to a large extent, the oxidation of other light hydrocarbons. The (111)- and (100)-terminated CeO_2 nanoparticles (nanooctahedra and nanocubes, respectively) have been chosen to support Ru nanoparticles. These two supports differ in the energy of the formation of oxygen vacancies, which is structure-sensitive, following the sequence (110) <(100) <(111) [8, 9]. The literature shows that it is impossible to synthesize ceria nanoparticles terminated by (110) faces only. Thus, cube-shaped ceria nanoparticles (terminated by highly reactive (100) faces) appear more suitable for catalytic applications than nanoparticles with irregular shapes or nanooctahedra (mainly terminated by (111) faces) [2]. However, the question about the effect of the type of the exposed surface of ceria (100 or 111) on Ru oxidation in oxygen-rich conditions (typical for VOCs oxidation) remains open. High oxygen mobility on (100) faces of ceria and associated with it good oxygen transport to Ru nanoparticles could make the realization of the MvK mechanism of C_3H_8 oxidation over Ru/CeO_2 easier but could also facilitate Ru oxidation to volatile RuO_4 — critical factor in Ru/CeO_2 deactivation.

In the present study, we will focus on the effect of the exposed surface of ceria support (111 vs 100) on Ru oxidation under actual conditions of C_3H_8 oxidation.

2. Experiment

Nanocubes (CeO_2(NC)) and nanooctahedra (CeO_2(NO)) of ceria were synthesized by the microwave-assisted hydrothermal method [10]. Briefly, $Ce(NO_3)_3$ was first dissolved in distilled water. Next, the obtained solution was mixed with an appropriate amount of aqueous sodium hydroxide (NaOH) solution (for cube-shaped crystals) or sodium phosphate (Na_3PO_4) solution (for octahedral-shaped crystals) and then stirred for 60 min. The final solution was treated at 200°C or 170°C for 3 h under autogenous pressure in an autoclave to obtain cube-shaped and octahedral nanocrystals, respectively. The as-obtained precipitate powder was washed and dried at 60°C for 12 h. Ru nanoparticles were deposited on the ceria nanocubes using a wet chemical deposition–precipitation method. Next, 250 mg of the ceria support was ultrasonically dispersed in 40 ml H_2O. Then, an appropriate amount of 11% Ru solution in HNO_3 was added to the ceria suspension to get 2.5 wt% Ru/CeO_2 catalyst and then ultrasonically treated for 10 min, dried at 60°C for 12 h, and annealed in H_2 at 500°C for 3 h.

The morphology of the samples was determined by scanning electron microscopy (SEM, FEI Nova NanoSEM 230) and transmission electron microscopy (TEM, Philips CM-20 SuperTwin instrument operating at 160 kV). The chemical composition in the samples was checked by energy-dispersive X-ray spectroscopy (EDS) using an FEI Nova NanoSEM 230 equipped with an EDAX Genesis XM4 detector.

The chemical composition of the catalysts under the reaction conditions of propane oxidation was studied by near-ambient pressure X-ray photoelectron spectroscopy (NAP-XPS). NAP-XPS measurements were performed using a laboratory NAP-XPS system (SPECS Surface Nano Analysis GmbH, Germany) equipped with a monochromated Al K_α X-ray source of high-intensity, a multichannel electron energy analyzer (SPECS PHOIBOS 150) coupled with a differentially pumped electrostatic prelens system. NAP-XPS spectra were acquired in the presence of 0.5 mbar of H_2 and 1 mbar of $C_3H_8+O_2$ (1 : 10) mixture in the temperature range from 25 to 500°C. The sample exposed to gasses was heated in a NAP cell through contact with a hot stage heated from the rear (vacuum) side by high-energy electron irradiation.

3. Results and discussion

Two types of ceria support for ruthenium nanoparticles were applied, i.e., nanooctahedra CeO_2(NO) and nanocubes CeO_2(NC) decored with Ru nanoparticles (NPs). Figure 1 shows

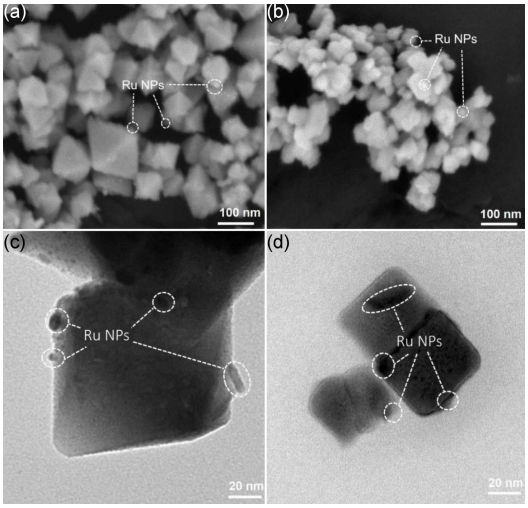

Fig. 1. Representative SEM and TEM images of as-prepared (a, c) Ru/CeO_2(NO) and (b, d) Ru/CeO_2(NC) samples, respectively.

the representative SEM and TEM images of Ru/CeO_2(NO) (Fig. 1a, c) and Ru/CeO_2(NO) (Fig. 1b, d) samples. EDS measurements show that Ru content in Ru/CeO_2(NO) and Ru/CeO_2(NC) was 2.50 wt% and 2.45 wt%, respectively. Thus, we conclude that Ru content in both samples was the same. As seen in Fig. 1a and c, the as-prepared Ru/CeO_2(NO) consists of $\sim$ 80–100 nm CeO_2 nanooctahedra decorated with Ru NPs a few nm in size. Figure 1b and d depicts an as-prepared Ru/CeO_2(NC) sample consisting of $\sim$ 50 nm CeO_2 nanocubes decorated with Ru NPs a few nm in size. Thus, it can be concluded that the differences in the behavior of Ru nanoparticles supported by CeO_2(NO) and CeO_2(NC) are limited mainly by the type of open face of the cerium support (100 vs 111), and not by the comparability of differences in the particle sizes of the cerium supports. The structure and morphology of CeO_2(NO) and CeO_2(NC) supports were studied in detail in our previous works [10–12]. It has been shown that CeO_2(NC) are single crystals, mainly ($> 90\%$) terminated by (100) faces, with a small ($< 10\%$) contribution of (110) and (111) faces at the edges and corners, respectively. CeO_2(NO) are single crystals mainly terminated by (111) faces.

Because the chemical state of the Ru species at the Ru/ceria interface is vital for the catalytic performance in the VOCs oxidation, which is typically performed at 473–773 K, the NAP-XPS study focuses on the temperature range from room temperature (RT) to 773 K. NAP-XPS Ru 3*d* spectra of the Ru/CeO_2(NO) and Ru/CeO_2(NC) catalysts are collected in Fig. 2a and Fig. 2b, respectively. The Ru 3*d* spectrum of both as-prepared samples exposed to 0.5 mbar of H_2 revealed the presence of Ru^0 only, which, according to the literature, exhibits the Ru $3d_{5/2}$ peak at binding energy (BE)

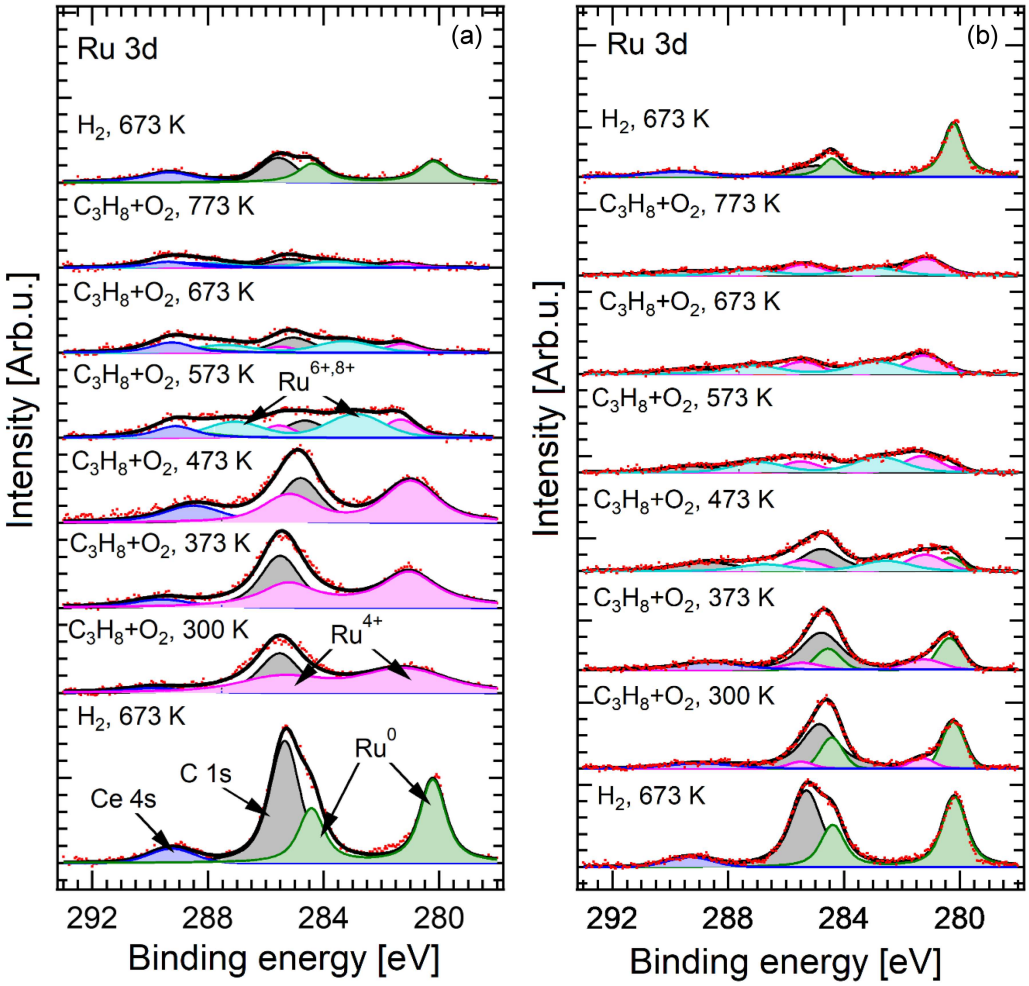

Fig. 2. NAP-XPS Ru 3*d* spectra collected for (a) Ru/CeO_2(NC) and (b) Ru/CeO_2(NO) catalyst in different environments (oxidative (C_3H_6+O_2 (1:10)), and reducing H_2 gas atmospheres) at different temperatures.

of about 280.5 eV [4, 13–15]. It should be noted that the Ru 3*d* spectrum overlaps with the C 1*s* peaks (285 and 289 eV) and Ce 4*s* (289.2 eV) signals, which complicates its analysis, especially in the case of air-exposed powder samples containing C-contamination.

NAP-XPS examination of the samples exposed to the oxygen-rich $C_3H_8 + O_2$ gas mixture showed ruthenium oxidation to higher oxidation states. As seen in Fig. 1a, the exposition of the Ru/CeO_2(NC) sample to the C_3H_8+O_2 gas mixture at 300 K and 473 K results in almost complete oxidation of ruthenium to RuO_2 form. It corresponds well with our previous NAP-XPS data for Ru NPs supported with irregularly shaped ceria nanoparticles, showing that ruthenium easily oxidizes in an O_2-rich environment even at room temperature [7]. Also, it shows that under VOCs oxidation over Ru-based catalysts, where a significant excess of oxygen is used, and the characteristic temperature range above 300°C, most of the ruthenium oxidizes to higher oxidation states — RuO_3 and RuO_4. Indeed, increasing the temperature to 573 K results in the appearance of the additional Ru 3*d* doublet, with the main (Ru $3d_{5/2}$) peak at about 283.5 eV, corresponding to RuO_x ($x > 4$) [16–18]. In contrast, the stepwise heating of the Ru/CeO_2(NO) showed slower oxidation of the Ru NPs in the C_3H_8+O_2 gas mixture (Fig. 2b). The comparison of Fig. 2a and Fig. 2b shows that Ru NPs oxidation in Ru/CeO_2(NO) remained metallic at lower (300–373 K) temperatures and started transforming into the RuO_x states only after heating to 473–573 K.

In both samples, increasing the temperature to 673 K and 773 K leads to the disappearance of the Ru-related XPS signal due to the volatile RuO_x formation. However, greater Ru disappearance takes place for Ru NPs supported by CeO_2(100). The decrease in the Ru-related XPS signal compared to the initial level for Ru/CeO_2(NC) and Ru/CeO_2(NO) is approximately 4 and 2 times, respectively.

Differences in Ru disappearance degree between Ru/CeO_2(NO) and Ru/CeO_2(NC) samples could be rationalized by the different abilities of ceria nanocubes and nanooctahedra to transport oxygen to Ru NPs. Density functional theory (DFT)

calculations by Nolan et al. [19] show that oxygen vacancy formation energies for (111), (110), and (100) surfaces and in the bulk of ceria are 2.60, +1.99, +2.27, and +3.39 eV, respectively. Taking into account that the energy of oxygen vacancy formation should strongly correlate with the ability to transport oxygen, we assume that the intensity of oxygen transport processes in ceria most probably follows the sequence bulk $\ll$ (111) $<$ (100). This assumption is in good agreement with molecular dynamics calculations by Castanet et al. [20], who calculated that the surface oxygen mobility on the (100) surface of CeO_2 is five orders higher than that on (111) surfaces. These theoretical data correspond well with the experimental atomic resolution TEM study of (111) and (100) faces of ceria by Lin et al. [21], which showed that the (111) surface is ideally truncated with an O termination, while the (100) surface has mixed terminations with Ce, O, and CeO on the outermost surface as well as the partially occupied atoms in the near-surface region. Mixed Ce and O termination in combination with low energy of oxygen vacancy formation makes favorable conditions for facile oxygen transport on (100) face of ceria. This hypothesis was confirmed experimentally by Bugnet et al. [22] using the in situ atomic resolution TEM technique, which directly shows a high ability for oxygen to diffuse over (100) surfaces of ceria. Summarizing the above-mentioned calculations and experimental studies, we assume that the high reactivity of (100) face of ceria is responsible for facile Ru oxidation to volatile RuO_4 when exposing the Ru/CeO_2 catalyst to an oxygen-rich atmosphere at the typical temperature window of VOCs oxidation.

From the point of view of practice, this process should have a noticeable impact on the stability of Ru/CeO_2-based catalysts. As seen before, the evaporation process of Ru from Ru/CeO_2(NC) catalyst in an oxygen-rich environment is more facile than that from Ru/CeO_2(NO) catalyst. Thus, it is logical to assume that despite the high activity of Ru/CeO_2(NC) structures [23], their stability in oxygen-rich conditions (typical for VOCs oxidation) is limited due to the facile loss of active phase (Ru) from the catalyst surface. However, the connection between Ru-evaporation and deactivation of catalytic activity of Ru/CeO_2 (111 vs 100) catalysts in VOCs oxidation needs more in-depth investigation, which will be performed in our future work.

4. Conclusions

The effect of the exposed surface of ceria support (111 vs 100) on Ru oxidation under realistic conditions of C_3H_8 oxidation was studied by the NAP-XPS technique. It has been shown that Ru NPs supported with ceria nanocubes (mainly terminated by (100) face) have a greater tendency to oxidize in oxygen-rich conditions of C_3H_8 oxidation than those supported with ceria nanooctahedra (mainly terminated by (111) face). This, in turn, results in lower thermal stability of Ru NPs supported with ceria nanocubes — high reactivity of (100) face of ceria facilitates ruthenium oxidation to the volatile RuO_4 form.

Acknowledgments

The authors thank Dr. D. Szymanski for EDS measurements. The authors would also like to thank the CERIC–ERIC consortium for financial support and access to the NAP-XPS facility.

References

[1] Y. Yang, S. Zhao, L. Cui, F. Bi, Y. Zhang, N. Liu, Y. Wang, F. Liu, C. He, X. Zhang, *Green Energy & Environment* **8**, 654 (2022).

[2] A. Trovarelli, J. Llorca, *ACS Catal.* **7**, 4716 (2017).

[3] J. Okal, M. Zawadzki, L. Krajczyk, *Catal. Today* **176**, 173 (2011).

[4] Z. Hu, Z. Wang, Y. Guo, L. Wang, Y. Guo, J. Zhang, W. Zhan, *Environ. Sci. Technol.* **52**, 9531 (2018).

[5] F. Ying, S. Wang, C. Au, S.-Y. Lai, *Gold Bull.* **43**, 241 (2010).

[6] S.K. Muhammad, A.R. Shaikh, M.H. Mohammad, *Atmos Environ.* **140**, 117 (2016).

[7] O. Bezkrovnyi, M. Vorokhta, M. Pawlyta, M. Ptak, L. Piliai, X. Xie, T.N. Dinhová, I. Khalakhan, I. Matolínová, L. Kepinski, *J. Mater. Chem. A Mater.* **10**, 16675 (2022).

[8] J.C. Conesa, *Surf. Sci.* **339**, 337 (1995).

[9] A. Demourgues, R.L. Neale, D.C. Sayle, U. Castanet, F. Caddeo, J.M. Flitcroft, R. Caygill, B.J. Pointon, M. Molinari, J. Majimel, *ACS Appl. Mater. Interfaces* **11**, 11384 (2019).

[10] O. Bezkrovnyi, P. Kraszkiewicz, M. Ptak, L. Kepinski, *Catal. Commun.* **117**, 94 (2018).

[11] O. Bezkrovnyi, P. Kraszkiewicz, W. Miśta, L. Kepinski, *Catal. Lett.* **151**, 1080 (2020).

[12] O. Bezkrovnyi, M.A. Małecka, R. Lisiecki, V. Ostroushko, A.G. Thomas, S. Gorantla, L. Kepinski, *CrystEngComm* **20**, 1698 (2018).

[13] K.A. Ledwa, L. Kępiński, M. Ptak, R. Szukiewicz, *Appl. Catal. B* **274**, 119090 (2020).

[14] D.J. Morgan, *Surf. Interface Anal.* **47**, 1072 (2015).

[15] C.L. Bianchi, V. Ragaini, M.G. Cattania, *Mater. Chem. Phys.* **29**, 297 (1991).

[16] T. Spătaru, L. Preda, P. Osiceanu, C. Munteanu, M. Marcu, C. Lete, N. Spătaru, A. Fujishima, *Electrocatalysis* **7**, 140 (2015).

[17] R. Liu, H. Iddir, Q. Fan et al., *J. Phys. Chem. B* **104**, 3518 (2000).

[18] Y. Park, B. Lee, C. Kim, Y. Oh, S. Nam, B. Park, *J. Mater. Res.* **24**, 2762 (2009).

[19] M. Nolan, J.E. Fearon, G.W. Watson, *Solid State Ion* **177**, 3069 (2006).

[20] U. Castanet, C. Feral-Martin, A. Demourgues, R.L. Neale, D.C. Sayle, F. Caddeo, J.M. Flitcroft, R. Caygill, B.J. Pointon, M. Molinari, J. Majimel, *ACS Appl. Mater. Interfaces* **11**, 11384 (2019).

[21] Y. Lin, Z. Wu, J. Wen, K.R. Poeppelmeier, L.D. Marks, *Nano Lett.* **14**, 191 (2014).

[22] M. Bugnet, S.H. Overbury, Z.L. Wu, T. Epicier, *Nano Lett.* **17**, 7652 (2017).

[23] Z. Wang, Z. Huang, J.T. Brosnahan, S. Zhang, Y. Guo, Y. Guo, L. Wang, Y. Wang, W. Zhan, *Environ. Sci. Technol.* **53**, 5349 (2019).